Influence of Different Direct Cooling Systems on Interior Permanent Magnet Traction Machine Performance

Anaugh Banerjee , WMG, University of Warwick ,Coventry , UK , anaugh.banerjee@warwick.ac.uk

Juliette Soulard , WMG , University of Warwick , Coventry, UK , J.Soulard@warwick.ac.uk

Xiyun Ma , WMG , University of Warwick , Coventry , UK , Xiyun.Ma@warwick.ac.uk

Sreeju S Nair , R&D Pwowertrain , TVS Motor Company , India , S.SreejuNair@tvsmotor.com

SP Senthilnathan , Vehicle Systems , TVS Motor Company , India , Senthil.nathan@tvsmotor.com

***Abstract*—This paper investigates the impact of direct cooling systems on a 3-phase 12 slot/10 pole, 30kW interior permanent magnet machine for electric two-wheeler applications. Both in-slot oil cooling and shaft spray cooling models have been developed, allowing to compare with an air-cooling system in terms of continuous torque-speed envelopes and drive cycle efficiency. Multi-domain simulations have been carried out using Ansys Motor-CAD. It is found that the best continuous performance is obtained by shaft spray cooling and the in-slot oil cooling on its own is the least attractive. The combination of in-slot oil cooling and air cooling shows a significantly better performance than air cooling but the gain in the continuous torque may not justify the design and manufacturing complexity associated with it.**

Keywords—electric motor, direct cooling, oil cooling, permanent magnet machine, electric two-wheeler.

I. INTRODUCTION

An electric motor for transportation generally requires high power density, high constant power speed range, high efficiency, low cost, and high-volume manufacturing. Out of the various machines used as traction motors for EVs, the interior permanent magnet motor (IPM) is one of the most promising motor types which is used by most of the automotive manufacturers. Permanent magnets provide high torque density and/or high-power density, and flexibility in design for achieving the desired performance utilizing reluctance torque. But it also comes with the drawback of having the risk of irreversible demagnetization at high temperatures, usage of negative d-current for flux weakening at high speeds, reducing efficiency [1] [2].

For a traction motor, both peak and continuous performance are important since they define the acceleration and efficiency on drive cycles of the vehicle, respectively. The peak performance of a motor is linked to the inverter maximal current, and voltage and the motor may only be able to work at these working points for a short duration depending on thermal history. The continuous torque or power is limited by the thermal behavior of the motor combined with its cooling system, keeping critical materials in the stator and rotor within their maximal temperature limits.

Electromagnetic and mechanical losses in the different components of the motor create heat flux from where they are created to the cooling system keeping certain parts at a lower temperature. By keeping temperatures under control, a better cooling system allows to reduce stator winding losses on drive cycle and increase the lifetime of the electric machine, reducing risk for winding failure. The remanence and coercivity of NdFeB permanent magnets reduce with temperature. Poor or faulty cooling can cause partial or full demagnetization of the magnets [3].

The cooling system primarily impacts the continuous performance of the motor, maximal torque as function of speed or power as function of speed at given temperature limits. Natural convection or forced air cooling, and liquid cooling (using water jacket or oil) are the commonly used methods in electric machines. The stator winding losses account for most of the losses at high torque conditions. Therefore, direct cooling solutions extracting winding losses are receiving attention to tune the ratio of peak to continuous torque.

In-slot (direct) cooling between the coils in a double-layer concentrated non-overlapping winding machine was investigated in [4]. With the use of flat wires, a current density of 20 A/mm² has been achieved along with the combination of direct cooling. A direct water-cooled design by winding a steel pipe carrying the coolant for 205 kW machine used for a bus application. The developed and tested prototype reported a maximum current density of 14A/mm² at 2 L/min coolant flow rate [5]. Another double-layer concentrated winding machine with in-slot cooling and round wires achieved a peak power of 60 kW and could operate at current densities of 35A/mm² for 30 s and 25A/mm² continuously with a power density of 8kW/L and a peak efficiency of 94 % [6]. With the proposed solution, the machine can achieve a significantly lower winding temperature and gain in efficiency between 1.5 % and 3.5% on different drive cycles compared to water jacket cooling. Oil spray cooling can directly extract heat from end windings as reported in [7- 9].

Doubled current density (23A/mm²) and a doubled power density were achieved with the help of spraying oil for a machine with hairpin windings [7]. An oil spray cooling concept with nozzle on the hollow shaft of an induction machine allowed a doubling of the continuous power of the motor [8]. The comparison of continuous power of an IPM motor with hairpin windings for a four-wheeler application with a continuous power range of 120 kW showed that the oil spray cooling provides the best continuous power over a wider speed range compared to the water-jacket-cooled motor [9].

Choice of cooling system also influences cost, packaging, and design complexity. Table I shows the motors used in different commercial two wheelers with different power levels. The low power motors as well as some medium powered vehicles like Zero DSR and Zero SRS used air cooling which could achieve only 42% to 50 % of the peak as continuous power [10], [11], [12] .While with oil cooling, the motor was able to achieve 87% of the peak as continuous power [13]. Unfortunately, the continuous to peak performance ratio with a water jacket could not be identified from the information in [14].

TABLE I.
COMPARISON OF ELECTRIC MOTORS USED IN ELECTRIC TWO-WHEELERS AT DIFFERENT POWER LEVELS.

Manufacturer	Peak power (kW)	Continuous power (kW)	Cooling method	Motor type
Soco TC Max [10]	5	3.9	Air	-
Maeving RM1 [11]	4.4	3.0	Air	-
Zero DSR[12]	52	22	Air	IPM
Zero SRS [12]	82	40	Air	IPM
Energica Ego+ [13]	126	110	Oil	IPM
Harley-Davidson Lightwire One [14]	75	-	Water Jacket	IPM

Based on the data in Table I, a specific 3-phase 12- slot/10-pole IPM motor design has been selected as the case study. This paper describes how to conduct a thorough investigation of advantages and drawbacks of direct oil cooling systems compared to air cooling. The electrical machine variants with comparable peak performance will be conducted in section II, followed by the investigated cooling systems, including air cooling, in-slot oil cooling system (ISOC), a combination of ISOC and air cooling (ISOC+air cooling) and shaft spray cooling (SSC) system in section III. In section IV, continuous torque-speed characteristics are derived and analyzed, including quantifying the influence of oil flow rate before looking on efficiency maps and performance on drive cycle. Conclusions are drawn in section V with manufacturing and cost considerations.

II. E-MACHINE SCALING

A. Initial machine design

Thermal and electromagnetic performance have different scaling relationship to dimensions since torque is linked to rotor volume and convective heat transfer is linked to area of contact surfaces.

The traction motor design investigated in [15] is taken as the starting point for the IPM with in-slot oil cooling. The design presents a suitable slot-pole combination allowing the inclusion of the cooling ducts in the stator yoke as well. The base motor has a peak torque of 140 Nm, base speed of 3600 rpm and peak power of 52 kW, with active length of 102 mm, and outer stator diameter 180 mm.

B. Scaled machine design and specifications

The machine for the case study is scaled down to a smaller volume due to the reduced maximal torque target (see Table II), using equations (1) and (2). The scaling is assuming the electromagnetic torque T_{em} is proportional to the alignment torque, which depends on the stator bore diameter (D), active length (L), number of turns per slot (n_s), phase current (I) , air gap flux density created by the magnets (B), electric loading (S), number of stator slots(Q_s), fundamental winding factor(k_w), and phase advance angle (β).

$$T_{em} = {}^{1}/_{4}\, SB\pi D^2 L k_w \sin\beta \quad (1)$$

$$S = Q_s(n_s I) / (\pi D) \quad (2)$$

The base speed of the motor is limited by the DC bus voltage of the motor. Design iterations were conducted to obtain the geometric parameters meeting the target torque as presented in Table II. The performance in Table II were calculated using ANSYS Motor-CAD, with assumption of stator winding and magnet temperatures of 150 °C and 120°C, respectively.

TABLE II.
MAIN DIMENSIONS AND FEATURES OF SCALED MOTOR

Slot number	12	DC bus voltage	385 V
Pole number	10	Phase RMS current (Peak)	130 A
Stator outer diameter	160 mm	Peak torque	78 Nm
Active length	110 mm	Peak power	30 kW
Airgap length	0.5 mm	Base speed	3900 rpm
Electrical steel grade	M235-35A	Maximum speed	12000 rpm
Magnet grade	N42UH		

TABLE III.
WINDING DEFINITIONS

	ISOC ISOC + Air cooling	SSC Air cooling
Wire diameter (mm)	0.99	0.99
No. of Strands	3	5
No. of turns/ coil	18	18
No. of parallel paths	2	2
Copper fill factor	0.21	0.35
Maximum. current density (A/mm²)	34	20.4

The winding design was modified for the ISOC and ISOC + air cooling as compared to air cooling and SSC (see Table III). For ISOC and ISOC + air cooling, the copper fill factor is low to free enough space in the slot for accommodating the cooling channels and using three strands. While for SSC and air cooling, the extra space which was initially used for the cooling channels allowed to add two more strands, using the same wire diameter.

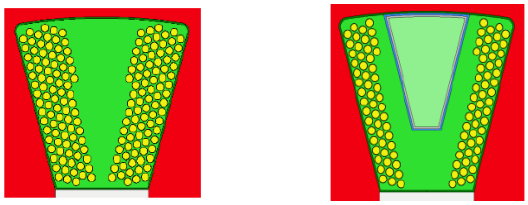

(a) (b)

Fig.1 Slot cross section with 18 turns per coil (a) 5 strands in hand for SSC and air cooling with copper fill factor of 0.35 (b) 3 strands along with the cooling channel for permitting the oil flow in ISOC and ISOC +air cooling with a copper fill factor of 0.21.

As the number of strands in the two designs are different with the same wire size, the phase resistance with 3 strands is 0.082 Ω, compared to 0.049 Ω with 5 strands, with current densities of 34 A/mm² and 20.4 A/mm², respectively. The slot cross sections of both designs can be seen in Fig.1

III. INVESTIGATED COOLING SYSTEMS

To tune the continuous performance of the motor, at given peak performance, several cooling systems have been considered, such as air cooling, in-slot oil cooling (ISOC), a combination of ISOC and air cooling, as well as shaft spray cooling.

A. Air cooling

This is the simplest cooling system which uses the ambient conditions for the heat transfer, including radial fins with a length of 10 mm and thickness of 2 mm on the outside of the housing (see Fig. 2). For a traction motor used in two-wheeler applications, the incoming flow of air when the vehicle moves can be considered as a forced air cooling conditions. Ambient temperature of 60°C and air flow rate proportional to the speed of the motor were assumed.

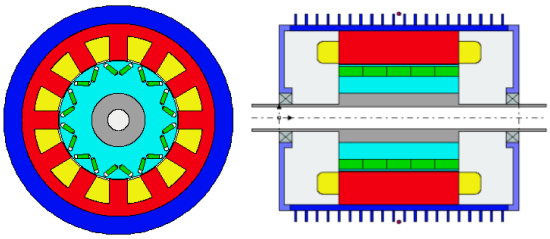

Fig.2 Radial and axial cross-sectional views of the motor with radial fins for air cooling.

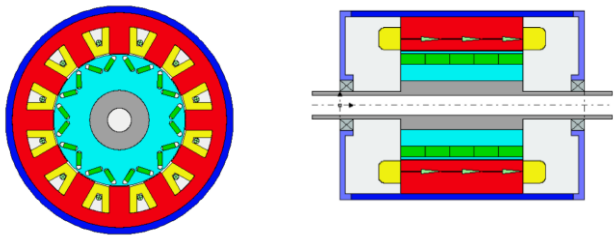

Fig.3 Radial and axial cross section of the motor with in-slot oil cooling (ISOC). The flow of oil is parallel to the axis of the rotation.

B. In-slot oil cooling (ISOC)

In this cooling system design, a cooling channel has been placed in the slot. Oil has been chosen as the coolant medium. Oil being an electrical insulator, any leakage with oil encountering the windings would not be hazardous, assuming compatibility of oil with insulation system has been confirmed. The flow of oil is parallel to the axis of rotation as shown in Fig.3 and the oil flows through each of the channels separately. For better conduction of the heat from the winding to the channels, the potting material Lord Cooltherm EP 200 having a thermal conductivity of 2 W/m-K was selected as an impregnation medium. The boundary conditions used for the simulations are presented in Table IV. The ambient temperature is kept at 60°C with a constant oil flow rate and the simulations were carried out at the peak current and base speed for 120 seconds. The heat transfer coefficient (HTC) between the slot cooling channel and the slot area with the potting material is 260.6 W/m²/°C, when simulating at the peak operating conditions.

TABLE IV.
BOUNDARY CONDITIONS FOR THERMAL SIMULATION OF THE MOTOR WITH ISOC AND ISOC+AIR COOLING

Oil type	Mobil Jet Oil II
Inlet oil temperature	60°C
Current density	34 A/mm2
Oil flow rate	8 L/min
Oil thermal conductivity	0.148 W/m-K
Cooling channel dimension (width x height)	14 mm x 7.5 mm

C. In-slot oil cooling (ISOC) + air cooling

In addition to the ISOC, the housing of the motor has the same fins as air cooling case (see Fig.4) so that this design has a combination of oil cooling and air cooling. The boundary conditions used for the simulation are shown in Table IV and the air flow is assumed to be proportional to the speed.

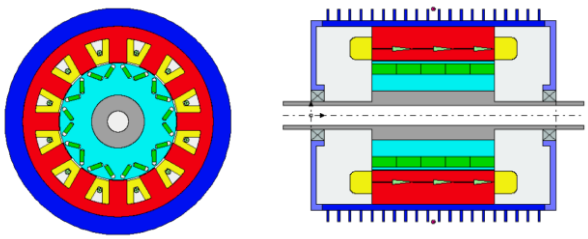

Fig.4 Radial and axial cross section of the motor with ISOC + air cooling.

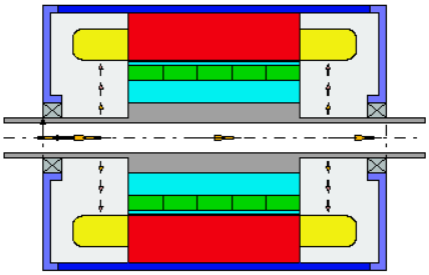

Fig.5 Axial cross section of the motor with the shaft spray cooling system.

D. Shaft Spray Cooling (SSC)

The shaft spray cooling system uses nozzles on the surface of the hollow shaft to spray oil onto the inside diameter of the end windings when the shaft rotates (see Fig.5). The nozzles have a diameter of 2.5 mm. For this cooling system, the end winding overhang was increased from 25 mm to 36 mm. This design choice will be justified in section IV. For both SSC and air cooling, vacuum pressure impregnation method has been considered as the chemical compatibility of the oil with the potting material has not been investigated. The flow rate of 8 L/min at an inlet temperature of 60°C with peak current and base speed for 120 s was estimated to lead to a heat transfer coefficient of 234 W/m²/°C for the oil spray on the end winding.

IV. Impact of Cooling Systems on Motor Performance

A. Impact on continuous performance

The continuous performance of the motor is the result of a coupling between the electromagnetic performance limited by inverter ratings combined with the thermal limits introduced by the materials used in the stator and the rotor to guarantee expected lifetime. By developing the thermal models with the boundary conditions as mentioned in Section III, the continuous performance is calculated with iterations between the electromagnetic and thermal models until convergence is reached. The simulation is carried out with a maximum magnet temperature of 150 °C (UH class) and stator winding temperature of 150°C (with insulation of IEC class 155).

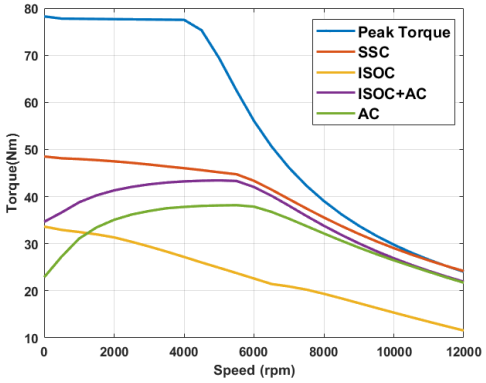

Fig.6 Comparison of peak and continuous torque-speed characteristics between different cooling systems.

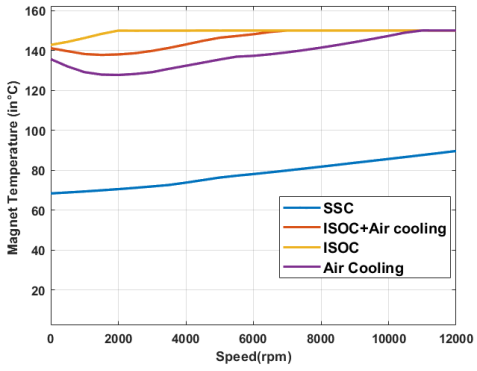

Fig.7 Comparison of magnet temperature variation in continuous operation with different cooling systems.

Fig.6 illustrates that the SSC gives a significantly higher continuous torque at lower speeds, due to the high heat transfer by the direct contact of the oil spray onto the end windings. The magnet temperature shown in Fig. 7 for SSC remains far away from the limiting temperature. This might seem that the magnet is under-utilized, but it provides a safety margin for the risk of demagnetization by winding or inverter short circuit. At lower speeds up to 2000 rpm, the ISOC shows a slightly higher performance than air cooling (Fig.6). ISOC shows the least performance with a linear decrease of the continuous torque values

with speed. The heat from the winding is transferred through the low thermal conductivity potting material before reaching the oil passing through the cooling channel. Around 2000 rpm, the magnet reaches its max. temperature limit of 150°C. With the magnet reaching the temperature limit at low speed, the remanent flux density of the magnet is reduced and thus the torque output also drops.

The ISOC when combined with air cooling shows a significant increase in the continuous performance as compared to ISOC only. The continuous torque increases up to around 6000 rpm as the air flow rate increases with speed. Air cooling shows a significant higher performance than ISOC only from 2000 rpm. However, ISOC + air cooling is better than ISOC only, or air cooling only, at all speeds.

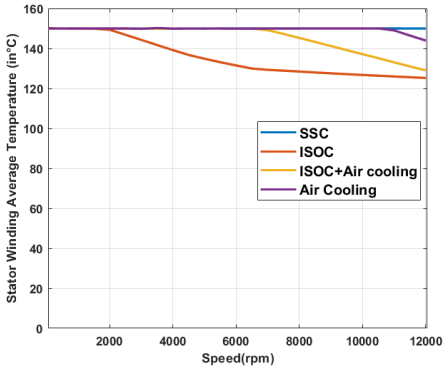

Fig.8 Comparison of average stator winding temperature variation in continuous operation with different cooling systems.

It should be noted that the air-cooling system is highly dependent on the external ambient conditions. For traction applications, the design of the vehicle is critical for allowing enough air flow into the motor housing. In a real-world drive application, a lower performance might be expected from air cooling since the assumption the force flow is proportional to the vehicle speed may not be valid.

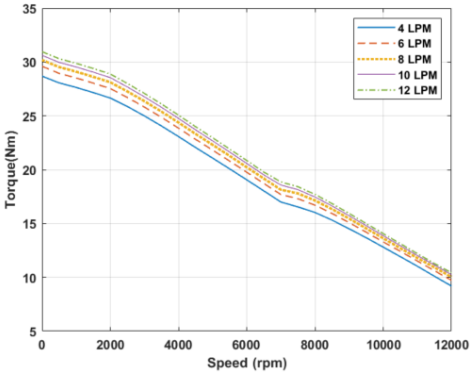

Fig.9 Impact of oil flow rate on the continuous torque speed characteristics of the motor with ISOC system

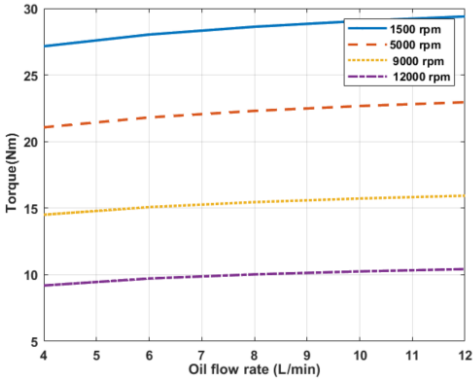

Fig.10 Impact of oil flow rate on the continuous torque at different speeds for the motor with ISOC system.

B. Impact of oil flow rate in ISOC

The ISOC, though having a cooling channel in the slot and being close to the winding the continuous performance, is not performing as expected, possibly due to the assumption the flow rate would be independent of the speed. The impact of the oil flow rate on the continuous torque was quantified and is shown in Fig.9. The continuous torque at given speed increases with the flow rate, but the influence is limitied. The maximum continuous torque at zero speed is 32 Nm at 12 L/min oil flow rate and the minimum torque value is 28 Nm at 4 L/min oil flow rate.

TABLE V.
CONTINUOUS TORQUE VALUES WITH ISOC AT DIFFERENT OIL FLOW RATES

Speed (rpm)	Torque (Nm) @4 L/min	Torque (Nm) @12 L/min	Increase in Torque (%)
1500	27.15	29.39	8.25
5000	21.06	22.95	8.97
9000	14.5	15.93	9.86
12000	9.19	10.42	13.38

In Fig.10, the increase of continuous torque with the flow rate at different speeds is mainly obtained at higher speeds, with marginal influence of flow rate at lower speeds. The maximal and minimal values of the continuous torque are shown in Table V. The increase in the flow rate requires to raise the power consumption of the pump, depleting the battery from its energy. Therefore, it is likely there is an optimal torque output per auxiliary power consumption.

C. End winding overhang analysis of SSC

As described in section III, the end winding overhang was set to 36 mm for the SSC motor. If the end winding length is shorter, it can be expected that some of the oil may flow into the air gap leading to increased windage losses. A sensitivity study is performed at 130 Arms and at base speed of 3900 rpm for a duration of 120 s with the same thermal boundary conditions as mentioned in Section III. The variations in average stator temperature and stator copper losses with the end-winding length are shown in Fig.11.Longer end winding overhang decreases the temperature due to higher contact surface between winding and oil, with the copper losses decreasing as well though there is more material in the winding.

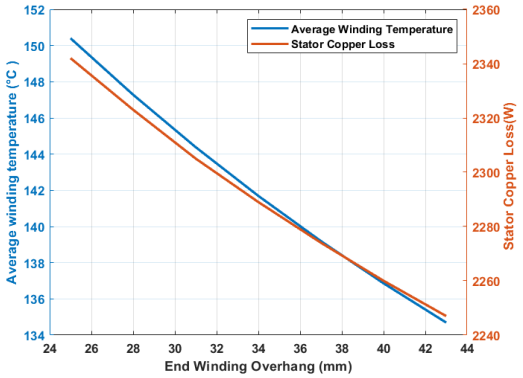

Fig.11 Variation of the average stator winding temperature and stator copper loss with different end winding overhang length @130Arms and 3900rpm.

The same investigation performed at a continuous operating point of 25 Nm and 6000 rpm showed that the copper loss at 25 mm overhang is 237.9 W and slightly decreases to 237.1 W at 43 mm overhang. At this working point, there is no significant increase in copper loss with a longer end-winding as during a long continuous operation, the copper losses generated become equal to the heat dissipated achieving a steady-state condition. Therefore, by increasing the winding overhang slightly for a better heat transfer and reducing the possibility of oil flow into the air gap can be more beneficial though longer end-winding would increase the cost of the electric machine and its weight.

D. Impact on drive cycle performance

The machine is simulated on a World Motorcycle Test Cycle (WMTC) drive cycle with different cooling systems for comparison and the average efficiency and losses along with the other machine features are presented in Table VI.

TABLE VI.
COMPARSION OF THE MACHINE FEATURES WITH DIFFERENT COOLING SYSTEMS

	Air Cooling	ISOC	ISOC+Air cooling	SSC
Peak current density (A/mm²)	20.4	34	34	20.4
Housing outer diameter (mm)	190	170	190	170
Winding weight (kg)	2.08	1.25	1.25	2.91
Active weight incl. housing (kg)	16.24	15.51	16.14	15.80
Continuous/ peak torque @3900 rpm	0.48	0.35	0.55	0.59
Power density (kW/L)	5.74	3.62	5.82	6.61
Specific power density @6000 rpm (kW/kg)	1.60	0.81	1.63	1.72
Average drive cycle efficiency (%)	93	91.6	92	93.3
Total losses per drive cycle (W)	74	92	91	70
Iron/total loss over the drive cycle (%)	77.3	67.3	66.8	87.3

The average drive cycle efficiency of the SSC is slightly higher than the air-cooling case while the ISOC and ISOC + air cooling have higher losses. Though the continuous performance of the SSC is significantly improved compared to air cooling, it does not translate into higher efficiency when compared. One of the prime reasons can be explained looking at Fig.12 showing the drive cycle points superposed on the efficiency map, with the continuous torque-speed characteristics visible as well. The drive cycle points are well within the continuous torque-speed envelop, in areas where the main losses are due to the iron losses

in the stator. Therefore, the housing with fins in the case of air cooling is a good solution. However, a drive cycle vehicle would benefit more from the higher continuous to peak torque ratio provided by the SSC solution.

The active volume and active weight include the stator housing and the end winding overhang. The SSC has the highest power density and specific power. The power density is obtained considering the continuous power delivered at 6000 rpm with different cooling systems. To complement the investigations, the mass and volume required by the oil cooling systems as well as the energy required to circulate the oil will be added in future work.

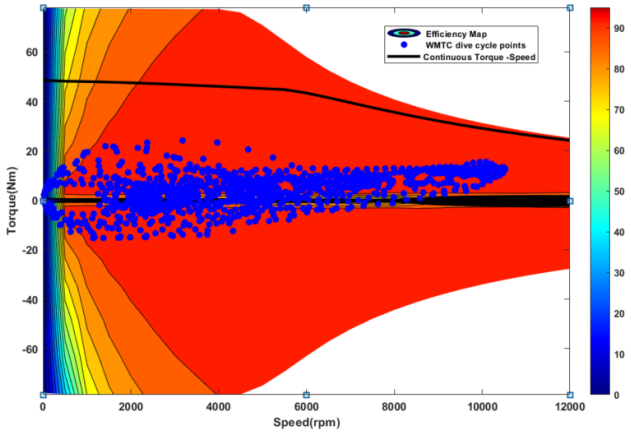

Fig.12 Efficiency map of the motor with the drive cycle data points and the continuous torque-speed envelope for the motor with SSC system.

V. CONCLUSION

This paper investigated the impact of different direct cooling systems on motor continuous performance with the same electromagnetic design, aiming for a higher continuous to peak performance ratio, relying on a better thermal behavior. Motor with shaft spray oil cooling achieved the highest continuous to peak performance ratio (0.59) at low speed as well as the highest specific power and the best efficiency on vehicle drive cycle. However, the study did not include the energy required by the oil cooling circulating pump. Introducing in-slot cooling reduces the copper fill factor, therefore it did not show significant gain in continuous performance, nor drive cycle efficiency. A combination of in-slot oil cooling and air-cooling system (fins on housing) managing stator iron losses would present better performance in terms of continuous torque but failed to improve the efficiency on drive cycle in the investigated case. Increased complexity of the e-machine and its cooling (adding components and auxiliary energy to be taken from the battery) along with the manufacturing complexity for introducing the channels into the stator slot may undermine the attractivity of the solution.

The described procedure illustrated by a case study allows to provide key information during selection of the cooling system most suited for an application with different peak continuous performance requirements. These investigations would take place before running optimization of the design and its chosen cooling system.

VI .REFERENCES

[1] Z. Q. Zhu, W. Q. Chu and Y. Guan, "Quantitative comparison of electromagnetic performance of electrical machines for HEVs/EVs," *CES TEMS* ,vol.1, no.1, pp. 37-47, Mar.2017.

[2] E. Agamloh, A. Jouanne and A. Yokochi, "An overview of electric machine trends in modern electric vehicles," *Machines*, vol. 8, no. 2, Apr. 2020.

[3] S. Ruoho, J. Kolehmainen, J. Ikaheimo and A. Arkkio, "Interdependence of demagnetization, loading, and temperature rise in a permanent-magnet synchronous motor," *IEEE Trans. Magn.*, vol. 46, no. 3, pp. 949-953, 09 Oct.2009 .

[4] M. Schiefer and M. Doppelbauer, "Indirect slot cooling for high-power-density machines with concentrated winding," *conf. IEMDC*, Coeur d'Alene, ID, USA, pp 1820-1825, 10-13 May 2015.

[5] P. Lindh, I. Petrov, J. Pyrhönen, E. Scherman, M. Niemelä and P. Immonen, "Direct liquid cooling method verified with a permanent-magnet traction motor in a bus," *IEEE Trans. Ind. Appl.,* vol. 55, no. 4, pp. 4183-4191,31 Mar. 2019.

[6] A.Acquaviva, "High performance cooling of traction brushless machines," Chalmers University of Technology, Ph.D thesis Gothenburg, Sweden, 2021.

[7] C. Liu *et al*, "Experimental investigation on oil spray cooling with hairpin windings," *IEEE Trans. Ind. Electron*, vol. 67, no. 9, pp. 7343-7353, 2020.

[8] B. Assaad, K. Mikati and T. V. Tran and E. Negre, "Experimental study of oil cooled induction motor for hybrid and electric vehicles,," *conf. XIII ICEM*, Alexandroupoli, Greece, pp. 1195-1200, 3-6 Sept. 2018.

[9] J.Gross, "Performance analysis of electric motor technologies for an electric vehicle powertrain," white paper, Motor Design Limited, 2019.

[10] "SuperSoco," 2023. [Online]. Available: https://supersoco.co.uk/.

[11] "Maeving Electric Motorcycles," [Online]. Available: https://maeving.com/.

[12] "Zero Motorcycles," [Online]. Available: https://zeromotorcycles.com/en-gb.

[13] "Energica Motorcycles," [Online]. Available: https://energicamotorcycles.co.uk/energica-models.

[14] "Harley Davidson Livewire," [Online]. Available: https://www.livewire.com/en-gb.

[15] A. Acquaviva, S. Skoog and T. Thiringer, "Design and verification of in-slot oil-cooled tooth coil winding PM machines for traction applications," *IEEE Trans . Ind. Electron.*, vol. 68, no. 5, pp. 3719 -3726, 5 May 2020.